Research in Astron. Astrophys. **2013** Vol. **13** No. **10**, 1141–1154
http://www.raa-journal.org *http://www.iop.org/journals/raa*

***R**esearch in*
***A**stronomy and*
***A**strophysics*

The clustering of QSOs and the dark matter halos that host them *

Dong-Yao Zhao, Chang-Shuo Yan and Youjun Lu

National Astronomical Observatories, Chinese Academy of Sciences, Beijing 100012, China; *lu.youjun1@gmail.com*

Received 2012 May 3; accepted 2012 May 28

Abstract The spatial clustering of QSOs is an important measurable quantity which can be used to infer the properties of dark matter halos that host them. We construct a simple QSO model to explain the linear bias of QSOs measured by recent observations and explore the properties of dark matter halos that host a QSO. We assume that major mergers of dark matter halos can lead to the triggering of QSO phenomena, and the evolution of luminosity for a QSO generally shows two accretion phases, i.e., initially having a constant Eddington ratio due to the self-regulation of the accretion process when supply is sufficient, and then declining in rate with time as a power law due to either diminished supply or long term disk evolution. Using a Markov Chain Monte Carlo method, the model parameters are constrained by fitting the observationally determined QSO luminosity functions (LFs) in the hard X-ray and in the optical band simultaneously. Adopting the model parameters that best fit the QSO LFs, the linear bias of QSOs can be predicted and then compared with the observational measurements by accounting for various selection effects in different QSO surveys. We find that the latest measurements of the linear bias of QSOs from both the SDSS and BOSS QSO surveys can be well reproduced. The typical mass of SDSS QSOs at redshift $1.5 < z < 4.5$ is $\sim (3-6)\times 10^{12}\ h^{-1}\ M_{\odot}$ and the typical mass of BOSS QSOs at $z \sim 2.4$ is $\sim 2\times 10^{12}\ h^{-1}\ M_{\odot}$. For relatively faint QSOs, the mass distribution of their host dark matter halos is wider than that of bright QSOs because faint QSOs can be hosted in both big halos and smaller halos, but bright QSOs are only hosted in big halos, which is part of the reason for the predicted weak dependence of the linear biases on the QSO luminosity.

Key words: black hole physics — galaxies: active — cosmology

1 INTRODUCTION

QSOs are probably powered by accretion onto massive black holes (MBHs; e.g., Salpeter 1964; Lynden-Bell 1969). QSO-like nuclear activities probably play important roles in shaping galaxies and lead to strong correlations between the masses of MBHs and properties of their host galaxies, as the star formation in galaxies may be regulated by the energy or momentum output from the nuclear activities (Silk & Rees 1998; Fabian 1999; King 2003; Murray et al. 2005). The statistical properties of QSOs, such as their luminosity function (LF) and spatial distribution, are important

* Supported by the National Natural Science Foundation of China.

tools to investigate the assembly history of MBHs and the relationships between MBHs, their host galaxies and dark matter halos, which may thus further provide crucial constraints on the formation and evolution of galaxies.

The QSO LFs have been extensively studied and estimated in the optical, X-ray and other bands based on various observations and surveys, such as the Two Degree Field QSO Redshift Survey (2QZ), the Sloan Digital Sky Survey (SDSS), and that by the Advanced Satellite for Cosmology and Astrophysics (*ASCA*), *Chandra*, *XMM-Newton*, *Swift*, etc. (e.g., Richards et al. 2006; Bongiorno et al. 2007; Croom et al. 2009; Ueda et al. 2003; Barger et al. 2005; La Franca et al. 2005; Ebrero et al. 2009; Hasinger 2008; Silverman et al. 2008; Yencho et al. 2009; Aird et al. 2010). These observations have revealed two important evolutionary features of the QSO population, i.e., cosmic evolution and the evolution of downsizing in QSOs (e.g., Hasinger 2008; Croom et al. 2009). The QSO LFs and the evolutionary features of QSOs have been frequently accounted for by physically motivated empirical and semi-analytic models (Hopkins & Hernquist 2006; Croton et al. 2006; Malbon et al. 2007; Somerville et al. 2008; Shen 2009). However, there is usually some degeneracy among the model parameters involved in the generation rate of QSOs and the luminosity evolution or light curve (LC) of individual QSOs, which are part of the reason that the QSO LFs can be fitted by models with quite different LCs.

The spatial clustering of QSOs, as a function of redshift and luminosity, is not only an important tool to measure the properties of galaxies that host a QSO and their associated dark matter halos, but also useful in estimating the lifetime of QSOs (e.g., Martini & Weinberg 2001; Haiman & Hui 2001). Observational measurement of QSO clustering has become practical in recent years due to large sky area surveys, such as 2QZ (Croom et al. 2004) and SDSS (York et al. 2000). The linear bias of QSOs, $b_{\rm Q}$, is defined as the square root of the strength of the QSO two-point correlation function relative to the two-point correlation function of the underlying matter distribution, and has been measured at a number of redshifts (e.g. Shen et al. 2007, 2009; Myers et al. 2007; da Ângela et al. 2008). These estimations, together with the QSO LFs, can also be used to put further constraints on both the relationship between the masses of MBHs and their host dark matter halos and the LC of individual QSOs (Shen 2009). Future accurate estimates of the QSOs' linear bias, as a function of both redshift and luminosity, should help to reveal the underlying physics of QSOs.

In this paper, we construct a simple QSO model to explain the linear bias of QSOs measured by current observations and explore properties of a dark matter halo that hosts a QSO. The QSO model is based on the major merger hypothesis, i.e., major mergers of dark matter halos/galaxies can lead to nuclear activity right after the completion of the merger. The paper is organized as follows. In Section 2, we introduce a simple QSO model by adopting the major merger hypothesis and using parameterized LCs according to simple arguments on the luminosity evolution of individual QSOs. In Section 3, we formularize the linear bias according to the QSO model. Using the simple QSO model, we first fit the QSO LFs in the hard X-ray (2−10 keV) band by using the Markov Chain Monte Carlo (MCMC) method to constrain the model parameters in Section 4.1, and further test the model by the optical LFs. Adopting the model parameters that best fit the QSO LFs, we then model the linear bias of QSOs by considering various selection effects in the QSO surveys in Section 4.2. We find that the observationally determined biases are well reproduced by the model, and we also obtain further constraints on the mass distribution of the host dark matter halos of QSOs. In Section 4.3 we discuss the potential relationship between the mass of MBHs and their host dark matter halos. Conclusions and discussions are given in Section 5.

Throughout the paper, we assume a ΛCDM cosmology with $\Omega_M = 0.3$, $\Omega_\Lambda = 0.7$, $\Omega_b = 0.046$, $\sigma_8 = 0.801$ and $h = 0.71$ in units of 100 km s^{-1} Mpc^{-1}.

2 A SIMPLE PHYSICAL MODEL

The evolution of QSOs can be described by the QSO LF, which is controlled by two underlying factors: (1) the generation rate of QSOs, and (2) the accretion history of MBHs and the luminosity

evolution of individual QSOs. The generation rate of QSOs can be described by the number density of MBHs with initial mass $M_{\bullet,\rm i}$ (or equivalently the final mass $M_{\bullet,\rm f}$, i.e., the MBH mass right after the quench of nuclear activity, given the accretion history of MBHs) that was triggered at $z_{\rm i}$, which is denoted as $\dot{G}(M_{\bullet,\rm i}; z_{\rm i})$ (or $\dot{G}(M_{\bullet,\rm f}; z_{\rm i})$). For a fixed mass to energy conversion efficiency ϵ, the accretion history of an MBH is equivalent to the evolution history of the QSO bolometric luminosity, which is denoted as $\mathscr{L}_{\rm bol}(z; M_{\bullet,\rm f}, z_{\rm i}) \equiv \mathscr{L}_{\rm bol}(\tau; M_{\bullet,\rm f})$, where $\tau = \int_z^{z_{\rm i}} |\frac{dt}{dz}| dz$ is the age of a QSO detected at redshift z but triggered at redshift $z_{\rm i}$. The growth rate of the MBH is then given by $\dot{M}_\bullet(z; M_{\bullet,\rm f}, z_{\rm i}) = \dot{M}_\bullet(\tau; M_{\bullet,\rm f}) \equiv (1-\epsilon)\mathscr{L}(\tau; M_{\bullet,\rm f})/\epsilon c^2$. The bolometric LF of QSOs is then given by

$$\frac{d\Phi(L_{\rm bol}, z)}{dL_{\rm bol}} = \int_z^\infty \left|\frac{dt}{dz_{\rm i}}\right| dz_{\rm i} \int dM_{\bullet,\rm f} \dot{G}(M_{\bullet,\rm f}; z_{\rm i}) \delta(L_{\rm bol} - \mathscr{L}_{\rm bol}(z; M_{\bullet,\rm f}, z_{\rm i})). \quad (1)$$

2.1 The Generation Rate of QSOs

Major mergers of galaxies and/or dark matter halos have long been believed to be responsible for the triggering of QSOs (i.e., the major merger hypothesis) (e.g. Hernquist 1989; Carlberg 1990; Kauffmann & Haehnelt 2000), although other mechanisms, such as the secular evolution of stellar disks and minor mergers may also play a role in triggering nuclear activities (Greene et al. 2008). In this paper, we adopt the merger hypothesis and assume that major mergers of dark matter halos can lead to nuclear activity immediately after the completion of the halo merger. Under this assumption, the generation rate of QSOs is determined by the merger rate of dark matter halos and the relationship between the final MBH's mass and the halo's mass.

According to the Millennium and Millennium II simulations (Fakhouri & Ma 2008; and Fakhouri et al. 2010), the merger rate of halos can be described by a universal form with dependence on the mass ratio x, the resulting mass of the merged halos $M_{\rm H}$ and the redshift z (see also Genel et al. 2008, 2009). For those halos with mass $M_{\rm H}$, the mean merger rate R (in units of mergers per halo with mass $M_{\rm H}$ per unit redshift per unit progenitor mass ratio) can be fitted by

$$R(M_{\rm H}, x, z) = R_0 \left(\frac{M_{\rm H}}{10^{12} M_\odot}\right)^\alpha x^\beta \exp\left[\left(\frac{x}{\tilde{x}}\right)^\gamma\right] (1+z)^\eta, \quad (2)$$

where the best-fit parameters $(\alpha, \beta, \gamma, \eta, R_0, \tilde{x})$ are $(0.133, -1.995, 0.263, 0.0993, 0.0104, 9.27\times10^{-3})$ from Fakhouri et al. (2010). We define the major mergers as those mergers with mass ratio $x \in (1/3, 1)$. If the lower limit on the mass ratio of major mergers is relaxed to $1/4$, the major merger rate increases by a factor of 1.32 but its dependence on the merged halo mass does not change, and therefore a smaller ϵ is required in order to fit the hard X-ray luminosity functions (HXLFs) and optical luminosity functions (OLFs) (see Section 4.1). Note that the major merger rates estimated from simulations may be smaller than those obtained from the extended Press-Schechter theory by a factor of 1.5–2 (see Fakhouri & Ma 2008; Fakhouri et al. 2010; Genel et al. 2008, 2009; and Parkinson et al. 2008).

Observations suggest that the mass of an MBH is probably tightly correlated with the mass of its host halo (Ferrarese 2002; Bandara et al. 2009) as well as the properties of its host galaxy (Gebhardt et al. 2000; Ferrarese & Merritt 2000; Tremaine et al. 2002). Using both numerical simulations and analytical arguments, Booth & Schaye (2010) have also shown that the masses of MBHs may be determined by the mass of their host halos. For a halo with mass $M_{\rm H}$ that follows the Navarro-Frenk-White (NFW) density profile, on average the mass of the central MBH is

$$\langle \log M_{\bullet,\rm f} \rangle \propto \log\left[f(c,y)(1+z)^{1/3} {M_{\rm H}}^{5/3}\right], \quad (3)$$

where c is the halo concentration, $y \equiv r_{\rm ej}/r_{\rm vir}$, $r_{\rm ej}$ is the physical scale over which the MBH self-regulation takes place, $r_{\rm vir}$ is the virial radius, and

$$f(c,y) = \frac{c}{[\ln(1+c) - c/(1+c)]^2} \times \left(1 - \frac{1}{(1+cy)^2} - \frac{2\ln(1+cy)}{1+cy}\right). \quad (4)$$

The halo concentration is given by $c = A(M_{\rm H}/M_{\rm pivot})^B(1+z)^C$, $M_{\rm pivot} = 2\times10^{12}\ h^{-1}\ M_\odot$, $A = 5.71$, $B = -0.084$ and $C = -0.47$ from Duffy et al. (2008). Booth & Schaye (2010) find that $y = 0.22$ matches their simulation results with the observational relation obtained by Bandara et al. (2009). Setting a slightly smaller (or larger) y results in a smaller (or larger) $f(c,y)$ but an insignificant change in the shape of $f(c,y)$ as a function of c, which means the change can be compensated by the change in the normalization of the $M_{\bullet,\rm f} - M_{\rm H}$ relation.

Recent observations suggest that the central galaxy's stellar mass is proportional to the halo mass to the power of $\sim 1/3$ for the most massive halos, which indicates that massive galaxies and probably their central MBHs also grow slowly in the most massive halos, although their host halos grow rapidly (Brown & the Boötes Field Collaborations 2010). Considering this, we adopt a modified form for the relation between the mass of the MBH and the properties of the halo as

$$\langle \log M_{\bullet,\rm f}\rangle = \log\left[\frac{\mathscr{B}(1+z)^{1/3}f(c,y)}{\left(\frac{M_{\rm H}}{M_z^*}\right)^{-5/3}+\left(\frac{M_{\rm H}}{M_z^*}\right)^{-1/3}}\right], \tag{5}$$

where $M_z^* = 2M_0^*/[(1+z)/(1+z_{\rm turn})]^{\alpha_1} + [(1+z)/(1+z_{\rm turn})]^{\alpha_2}$, and $\mathscr{B}$, M_0^*, α_1, α_2 and $z_{\rm turn}$ are free parameters that may be constrained by observations. If $M_{\rm H} \ll M_z^*$ at $z \sim 0$, we have $\langle \log M_{\bullet,\rm f}\rangle \propto 5/3 \log M_{\rm H}$, which is consistent with what is estimated for the MBHs in nearby galaxies (Ferrarese 2002). Equation (5) gives the average mass of MBHs in halos with mass $M_{\rm H}$, but the real masses of MBHs may scatter around this mean value. In this paper, we assume that the distribution of the real MBH masses around the mean value, i.e., $P(\log M_{\bullet,\rm f}|\langle \log M_{\bullet,\rm f}\rangle)$ is a Gaussian distribution with mean $\langle \log M_{\bullet,\rm f}\rangle$ given by Equation (5) and a standard deviation of $\sigma_{\log M_\bullet - \log M_{\bullet,\rm f}}$. Hereafter we adopt a standard deviation of 0.3 dex in the MBH mass versus the halo mass relation, similar to that of the $M_\bullet - \sigma$ relation and the $M_\bullet - M_*$ relation, where M_* is the stellar mass.

With the major merger rate of dark matter halos and the $M_{\bullet,\rm f} - M_{\rm H}$ relation described above, the generation rate of QSOs is given by

$$\dot{G}(M_{\bullet,\rm f}; z_{\rm i}) = \int_0^\infty F(M_{\rm H,i})\frac{P(\log M_{\bullet,\rm f}|\langle \log M_{\bullet,\rm f}\rangle)}{M_{\bullet,\rm f}\ln(10)}\frac{\mathcal{R}(M_{\rm H,i}; z_{\rm i})}{|dt/dz_{\rm i}|}\frac{dn(M_{\rm H,i}; z_{\rm i})}{dM_{\rm H,i}}dM_{\rm H,i}, \tag{6}$$

where the halo mass function $\frac{dn(M_{\rm H,i};z_{\rm i})}{dM_{\rm H,i}}$ can be estimated through the fitting formula given by Sheth & Tormen (1999), and $F_{H,i}$ describes the fraction of major mergers that lead to nuclear activities and is given by

$$F(M_{\rm H,i}) = \exp\left[-\frac{M_{\rm cut,1}}{M_{\rm H,i}} - \frac{M_{\rm H,i}}{M_{\rm cut,2}}\right], \tag{7}$$

where $M_{\rm cut,1} = 3\times10^{11}M_\odot\ h^{-1}$ and $M_{\rm cut,2} = 10^{12}M_\odot\ h^{-1}(1+z)^{3/2}$.

2.2 The Light Curve and Luminosity Evolution of Individual QSOs

The growth of MBHs probably experiences two different phases (e.g., Small & Blandford 1992; Yu & Lu 2004, 2008). In the first phase, the disk accretion is self-regulated and close to the Eddington limit because the supply of gaseous material for the central MBHs to accrete is plentiful right after the nuclear activities start being triggered. The accretion rate in this phase is assumed to be a constant fraction of the Eddington limit, i.e., $\lambda_0\dot{M}_{\rm Edd}$, where $\dot{M}_{\rm Edd}$ is the Eddington rate and λ_0 is a constant. In the second phase, the QSO luminosity is approximated as a power law decay with time because of the decline of the supply and/or the long term evolution of disk accretion (Yu et al. 2005; Hopkins & Hernquist 2006; Yu & Lu 2008). The accretion is terminated once the luminosity declines by a factor of 1000 from the peak luminosity at which time its mass growth is insignificant, even over a Hubble time.

Assuming that a QSO detected at redshift z (or time t) is triggered due to a major merger experienced by its host halo at an earlier redshift $z_{\rm i}$ (or time $t_{\rm i}$), the age of the QSO is $\tau = \int_z^{z_{\rm i}} \left|\frac{dt}{dz'}\right| dz'$ and the mass of the MBH is $M_{\bullet,\tau}$ (or $M_{\bullet,{\rm i}}$) at z (or $z_{\rm i}$). The peak luminosity of the QSO during its evolution is reached at time $t_{\rm p}$ (or redshift $z_{\rm p}$) which corresponds to age $\tau_{\rm p} = \xi\tau_{\rm S}$, where $\tau_{\rm S} = 4.5\times10^8\lambda_0^{-1}\frac{\epsilon}{(1-\epsilon)}$ yr is the Salpeter timescale. After time $t_{\rm p}$, the luminosity of the QSO declines following a power law, i.e. $((\tau+\zeta\tau_{\rm S}-\tau_{\rm p})/\zeta\tau_{\rm S})^{-\gamma}$, where ζ and γ are free parameters which determine how fast the luminosity declines. The light curve (or luminosity evolution) of individual QSOs can be described as

$$\mathscr{L}_{\rm bol}(M_{\bullet,{\rm f}},\tau) = \lambda L_{\rm Edd}(M_{\bullet,\tau})\,, \tag{8}$$

where

$$\lambda = \begin{cases} \lambda_0, & \text{for } 0<\tau\le\tau_{\rm p}\,,\\ \lambda_0\dfrac{\left(\frac{\tau+\tau_{\rm D}-\tau_{\rm p}}{\tau_{\rm D}}\right)^{-\gamma}}{1+\frac{\zeta}{\gamma-1}\left[1-\left(\frac{\tau+\tau_{\rm D}-\tau_{\rm p}}{\tau_{\rm D}}\right)^{1-\gamma}\right]}, & \text{for } \tau_{\rm p}<\tau\le\tau_{\rm p}+\eta\tau_{\rm D}\,,\\ 0, & \text{for } \tau>\tau_{\rm p}+\eta\tau_{\rm D}\,, \end{cases} \tag{9}$$

and where $\tau_{\rm D} = \zeta\tau_{\rm S}$, and $\eta\tau_{\rm D} = (10^{3/\gamma}-1)\tau_{\rm D}$ is the duration of the second phase. Current observations show that the Eddington ratio of bright QSOs may scatter around a constant value close to 0.3 (Kollmeier et al. 2006 and Shen et al. 2007). According to these observations, we adopt a fixed Eddington ratio of $\lambda_0 = 0.3$ at the first accretion phase in this paper. Hereafter, we adopt $\epsilon = 0.1$ and $\gamma = 1.3$ according to Yu & Tremaine (2002), Yu & Lu (2004, 2008) and Yu et al. (2005).

2.3 QSO Luminosity Function at a Given Band

With the LC and the generation rate of QSOs described in Sections 2.1 and 2.2, the QSO bolometric LF can be obtained from Equation (1). However, QSO surveys are usually conducted at a specific band or several given bands, and the majority of the observationally determined QSO LFs are given in either the optical band or the X-ray band. To constrain the model parameters, it is necessary to derive the QSO LFs at the same band as that of the observations. For a given band Y, we define the bolometric correction (BC) as $C_Y \equiv L_{\rm bol}/\nu L_\nu|_{\nu=Y}$, where $\nu L_\nu|_{\nu=Y}$ is the monochromatic luminosity at the central frequency of the Y-band. In principle, C_Y may depend on the physical quantities like $L_{\rm bol}$, $M_\bullet$ and/or λ, and the value of C_Y for any given QSO could be distributed around a mean value given by the dependence of C_Y on the above quantities. With the BC for a band Y, the QSO LF at this band is

$$\frac{d\Phi(L_Y,z)}{dL_Y} = \iiint_z^\infty \dot{G}(M_{\bullet,{\rm f}};z_{\rm i})\delta(L_Y-\mathscr{L}_Y(z;M_{\bullet,{\rm f}},z_{\rm i}))P(\log C_Y|\langle\log C_Y\rangle)\left|\frac{dt}{dz_{\rm i}}\right| dz_{\rm i}dM_{\bullet,{\rm f}}d\log C_Y\,, \tag{10}$$

where $\mathscr{L}_Y(z;M_{\bullet,{\rm f}},z_{\rm i}) = \mathscr{L}_{\rm bol}(z;M_{\bullet,{\rm f}},z_{\rm i})/C_Y$, $P(\log C_Y|\langle\log C_Y\rangle)$ is assumed to be a Gaussian distribution of $\log C_Y$ around the mean value $\langle\log C_Y\rangle$ for any given $L_{\rm bol}$ or λ, which may be obtained from observations.

According to Vasudevan & Fabian (2009), the BC in the hard X-ray (2 – 10 keV) band is dependent on the Eddington ratio λ. The BCs are fitted by a function of λ by Jin et al. (2012), i.e.,

$$\log C_{\rm X} = \begin{cases} 0.773\log\lambda + 2.004, & \text{if}\lambda\ge0.01\,,\\ 0.7, & \text{if}\lambda<0.01\,. \end{cases} \tag{11}$$

Considering the variation and other factors, we assign a standard deviation of 0.3 dex to the log-normal distribution of $C_{\rm X}$.

Hopkins et al. (2007) estimate the BC in the optical B-band by recalibrating the spectral energy distribution of QSOs and find that the BC is luminosity dependent. On average, the BC in the B-band

is given by

$$\langle \log C_{\rm B} \rangle = \log \left[c_1 \left(\frac{L_{\rm bol}}{10^{10} L_\odot} \right)^{k_1} + c_2 \left(\frac{L_{\rm bol}}{10^{10} L_\odot} \right)^{k_2} \right], \quad (12)$$

where $(c_1, k_1, c_2, k_2) = (6.25, -0.37, 9.00, -0.012)$. For any given $L_{\rm bol}$, $C_{\rm B}$ follows a lognormal distribution with a mean of $\langle \log C_{\rm B} \rangle$ and a standard distribution of $\sigma_{\log(L_{\rm bol}/L_{\rm B})} = \sigma_1 (L_{\rm bol}/10^9 L_\odot)^\beta + \sigma_2$, where $(\sigma_1, \beta, \sigma_2) = (0.08, -0.25, 0.06)$.

To model the optical QSO LF, it is necessary to consider the obscuration effect because only type 1 QSOs can be detected but type 2 may be missed in the optical QSO surveys due to obscuration. Both type 1 and type 2 QSOs can be detected by hard X-ray surveys. Hasinger (2008) investigates the intrinsic absorption properties of 1290 AGNs in the hard X-ray band and finds that the obscuration fraction decreases with increasing X-ray luminosity. According to the estimates obtained by Hasinger (2008), we find the obscuration fraction can be fitted by $f_{\rm obsc} = \frac{T_1}{T_1+T_2} = -0.226 \log \frac{L_{\rm bol}}{C_X} + 10.31$, where T_1 and T_2 are the number density of type 1 and type 2 QSOs at any given luminosity, respectively. This obscuration fraction should be added into the integration in Equation (10) when estimating the optical QSO LFs. Here the obscuration fraction is assumed to be independent of redshift for simplicity, though it is still being debated whether the obscuration fraction is redshift dependent or not.

Given the BCs and the obscuration fraction as above, the QSO LFs can be modeled in both the hard X-ray band and optical band according to Equation (10). The free parameters involved in the model are ($\mathscr{B}$, M_0^*, α_1, α_2 and $z_{\rm turn}$) and (ξ, ζ), respectively. The first five parameters ($\mathscr{B}$, M_0^*, α_1, α_2 and $z_{\rm turn}$) define the relationship between the final mass of an MBH and the mass of its host halo after merging and the last two parameters define the LC of individual QSOs and the mass evolution of MBHs.

3 CLUSTERING OF QSOS

The linear bias of those QSOs with luminosity L_Y at the Y-band and redshift z can be derived by averaging over their host halos in the framework of the above QSO model. In this model, QSOs are triggered by major mergers of dark matter halos, and the spatial clustering of QSOs is determined by the spatial clustering of their host dark matter halos (i.e., the halos that result from the mergers). For any halos with mass $M_{\rm H}$ at redshift z, Tinker et al. (2010) obtain a fitting formula for the linear bias, i.e.

$$b(\nu) = 1 - A \frac{\nu^a}{\nu^a + \delta_c^a} + B\nu^b + C\nu^c, \quad (13)$$

where $\nu = \delta_c / \Sigma(M_{\rm H}, z)$, $\delta_c = 1.686$ is the critical linear overdensity for the collapse of halos, $\Sigma(M_{\rm H}, z)$ is the linear rms density fluctuations in a sphere of mass M at redshift z, and the parameters (A, B, C) and (a, b, c) are functions of Δ, where Δ is the overdensity defined as the mean interior density relative to the background. Here we adopt $\Delta = 200$, which defines a radius separating the virialized region and the region of continuing infall in an $\Omega_m = 1$ universe (Lacey & Cole 1994; Eke et al. 1998). The values of those parameters can be obtained from table 2 in Tinker et al. (2010). We note here that alternative fitting formulae of the linear bias for dark matter halos are also given by Jing (1998), Sheth et al. (2001) and others.

The linear bias of those QSOs with luminosities in the range from L_Y to $L_Y + dL_Y$ at the Y-band can then be obtained by averaging over all their host halos with different masses (cf. Haiman & Hui 2001; Martini & Weinberg 2001; Lidz et al. 2006; Hopkins et al. 2008; Shen 2009; White et al. 2012), i.e.

$$\begin{aligned} b(L_Y, z) \;=\; & \left[\frac{d\Phi(L_Y, z)}{dL_Y} \right]^{-1} \iiiint_z^\infty b(\nu) P(\log M_{\bullet,\rm f} | \langle \log M_{\bullet,\rm f} \rangle) F(M_{\rm H,i}) \mathcal{R}(M_{\rm H,i}; z_{\rm i}) \frac{dn(M_{\rm H,i}; z_{\rm i})}{dM_{\rm H,i}} \\ & \delta(L_Y - \mathscr{L}_Y(z; M_{\bullet,\rm f}, z_{\rm i})) P(\log C_Y | \langle \log C_Y \rangle) dz_{\rm i} d\log M_{\bullet,\rm f} dM_{\rm H,i} d\log C_Y \,. \end{aligned} \quad (14)$$

Usually the linear biases estimated from observations are for those QSOs in a sample with magnitudes or luminosities brighter than a detection limit or in a given range. In order to compare with observations, therefore, we may also obtain the averaged bias $b(z)$ from the QSO model as

$$\bar{b}(z) = \left[\int_{L_{Y,\min}(z)}^{L_{Y,\max}(z)} dL_Y \frac{d\Phi}{dL_Y}\right]^{-1} \int_{L_{Y,\min}(z)}^{L_{Y,\max}(z)} dL_Y \frac{d\Phi}{dL_Y} b(L_Y, z)\,, \tag{15}$$

where $L_{Y,\max}(z)$ and $L_{Y,\min}(z)$ are the upper and lower limits on the luminosities of QSOs in the sample, respectively.

Considering the magnitude limit of a telescope at a given Y-band, represented by a low luminosity threshold $L_{Y,\min}(z)$ on the observable QSOs, the mass function for the host halos of the observable QSOs at redshift z is given by

$$\begin{aligned}\frac{d\Phi(M_{\rm H}, z; > L_{Y,\min}(z))}{dM_{\rm H}} &\simeq \frac{d\Phi(M_{\rm H,i}, z; > L_{Y,\min}(z))}{dM_{\rm H,i}} \\ &= \iiint_z^\infty \int_{L_{Y,\min}(z)} P(\log M_{\bullet,\rm f}|\langle\log M_{\bullet,\rm f}\rangle) F(M_{\rm H,i}) \mathcal{R}(M_{\rm H,i}; z_{\rm i}) \frac{dn(M_{\rm H,i}; z_{\rm i})}{dM_{\rm H,i}} \\ &\quad \delta(L_Y - \mathscr{L}_Y(z; M_{\bullet,\rm f}, z_{\rm i})) P(\log C_Y|\langle\log C_Y\rangle) dz_{\rm i} d\log M_{\bullet,\rm f} d\log C_Y dL_Y,\end{aligned} \tag{16}$$

where $M_{\rm H}$ represents the host halo mass at redshift z, $M_{\rm H,i}$ the host halo mass at redshift z_i, and we make the critical assumption that the mass of the QSO host dark matter halo does not increase significantly during the QSO phase, i.e., $M_{\rm H,i} \simeq M_{\rm H}$. Finally, the mass distribution of the QSO host dark matter halos can be obtained by

$$P(M_{\rm H}, z; > L_{Y,\min}(z)) = \frac{d\Phi(M_{\rm H,i}, z; > L_{Y,\min}(z))}{dM_{\rm H}} \left[\int P(M_{\rm H}, z; > L_{Y,\min}(z)) dM_{\rm H}\right]^{-1}. \tag{17}$$

4 MODEL RESULTS

4.1 Calibrating the QSO Model by the QSO LFs

It has been shown that the host galaxies of the QSOs with luminosities ($\gtrsim 10^{44.5}$ergs^{-1}) are commonly interacting systems at redshift $z > 1$ (e.g., Bahcall et al. 1997), which is consistent with the hypothesis that major mergers of galaxies and dark matter halos lead to the triggering of QSO phenomena. However, other processes, such as the secular evolution of stellar disks and minor mergers, may play important roles in triggering the QSO phenomena at low redshift $z \lesssim 1$ (Greene et al. 2008). Therefore, we use the QSO model described above to simultaneously fit the observationally determined HXLFs by Aird et al. (2010) only at high redshift bins of $(1.5, 2.0)$, $(2.0, 2.5)$ and $(2.5, 3.5)$. The model parameters of the best fit are ($\log \mathscr{B}$, $\log M_0^*$, α_1, α_2 and $z_{\rm turn}$)=(11.87, 14.22, 2.83, –0.48, 1.60) and (ξ, ζ)=(1.11, 0.03). (The detailed method of this fitting will be presented in a different paper.) The uncertainties in each model parameter can be obtained by marginalizing over other parameters, i.e., $\log B = 11.87 \pm 0.54$, $\log M_0^* = 14.22 \pm 0.34$, $\alpha_1 = 2.83 \pm 0.44$, $\alpha_2 = -0.48 \pm 1.20$, $z_{\rm turn} = 1.60 \pm 0.59$, $\log \xi = 0.044 \pm 0.15$ and $\log \zeta = -2.47 \pm 0.41$.

Figure 1 shows both the observationally determined HXLFs (Aird et al. 2010) and the model HXLFs that best fit the observations. As shown in Figure 1, the observations can be well fitted by the QSO model. Adopting the model parameters of the best fit, the QSO LFs in the B-band can also be estimated.

Figure 2 shows the optical QSO LF obtained from both observations (Richards et al. 2006; Bongiorno et al. 2007) and the above QSO model. Apparently the observations can be well matched by the QSO model that best fits the HXLFs. Hereafter, we will adopt these model parameters, calibrated by the HXLFs and OLFs, to estimate the linear biases of QSOs and study the dark matter halos that host them.

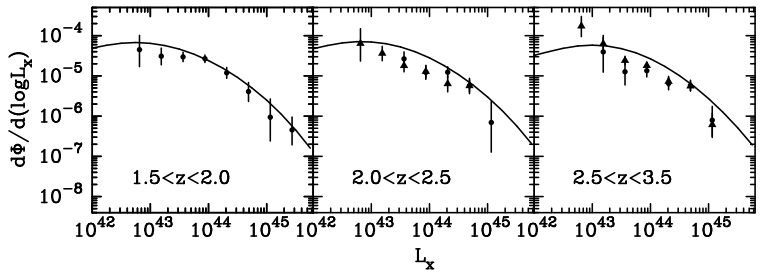

Fig. 1 The QSO LFs in the hard X-ray (2 – 10 keV) band. The circles and triangles both represent the estimates obtained from observations by Aird et al. (2010; see their fig. 9); The solid lines represent the QSO LFs obtained from the QSO model that best fit the observational data, and the model parameters of the best fit are ($\log \mathscr{B}$, $\log M_0^*$, α_1, α_2 and $z_{\rm turn}$)=(11.87, 14.22, 2.83, −0.48, 1.60) and (ξ, ζ) = (1.11, 0.003), respectively.

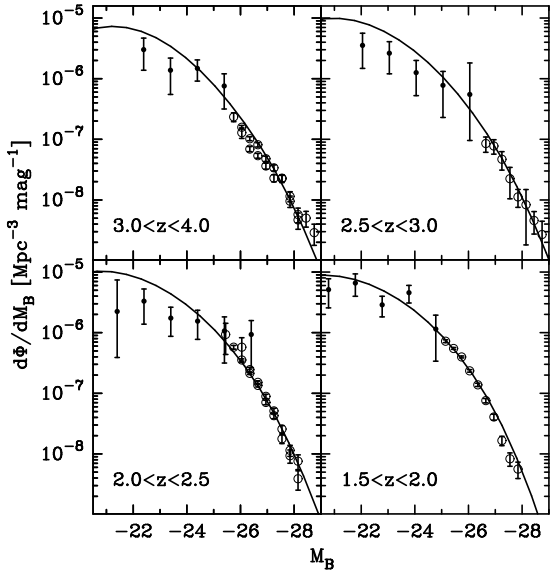

Fig. 2 The QSO LFs in the *B*-band. The filled and open circles represent the observationally determined LFs by Bongiorno et al. (2007) and Richards et al. (2006), respectively. The solid lines show the QSO LFs obtained from the QSO model that best fits the HXLFs.

4.2 The Linear Bias of QSOs

In the past several years, quite a number of estimates on the linear bias of QSOs have emerged in the literature, mainly due to the large sky area surveys, such as 2QZ, SDSS and BOSS. Figure 3 shows those latest estimates on the linear bias of QSOs, including those measured from SDSS by Ross et al. (2009; diamonds in the left panel) and Shen et al. (2009; circles in the left panel) and from BOSS by White et al. (2012; squares in the right panel). The QSO samples obtained from these surveys are magnitude limited, e.g., the QSOs in the SDSS sample are selected to an *i*-magnitude

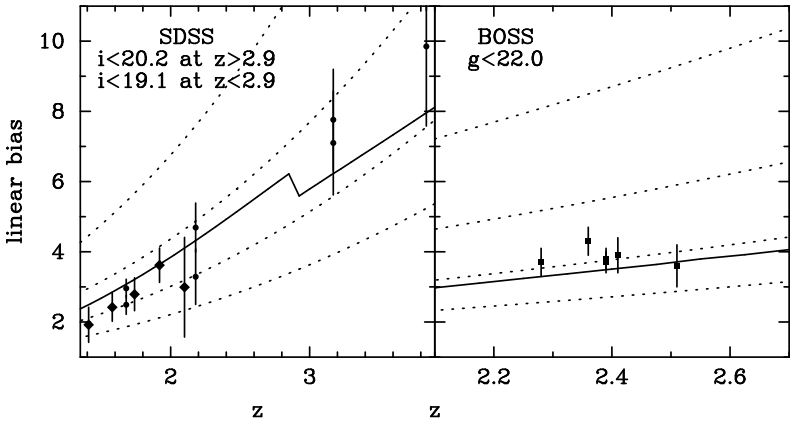

Fig. 3 The linear bias of QSOs at different redshifts. In the left panel, filled diamonds and circles are the linear biases for the QSOs in the Data Release 5 (DR5) Quasar Catalog estimated by Ross et al. (2009) and Shen (2009), respectively. In the right panel, the filled squares are the estimated linear biases of the QSOs discovered by BOSS (White et al. 2012). The solid lines are the biases predicted from the best fit QSO model by accounting for the flux limit of both surveys, i.e., the *i*-band magnitude limit for the DR5 QSOs is 19.1 at $z < 2.9$ and 20.2 at > 2.9; and the *g*-band magnitude limit for the BOSS QSOs is 22.0. Dotted lines from top to bottom show the expected linear bias of dark matter halos with mass $M_{\rm H} = 10^{13.5}\ h^{-1}\ M_\odot, 10^{13}\ h^{-1}\ M_\odot, 10^{12.5}\ h^{-1}\ M_\odot$ and $10^{12}\ h^{-1}\ M_\odot$, respectively.

limit of 19.1 at $z \leq 2.9$ and 20.2 at $z > 2.9$, while the QSOs in the BOSS sample are selected to a *g*-magnitude limit of 22. To compare with these measurements, it is necessary to account for the magnitude limits in the QSO model (see Eq. (15)). In the left (or right) panel of Figure 3, the solid curve shows the model results of the linear bias for the SDSS (or BOSS) QSOs by adopting the model parameters calibrated by the QSO LFs in Section 4.1. In general, the biases estimated from the QSO model are very consistent with the observational ones, though it appears that the model slightly underestimates the biases at high redshifts ($z > 3$; see the left panel of Fig. 3).

Figure 4 shows the mass distribution for the host dark matter halos of the SDSS QSOs (left panel) and the BOSS QSOs (right panel) obtained from our model according to Equation (16). The peaks of the halo mass distributions of the SDSS QSOs at different redshifts are $\log(M_{\rm H}/h^{-1}\ M_\odot) \sim 12.40-12.80$ at $z = 1.5-4.5$ (see the left panel of Fig. 4), and the logarithmic mean of the SDSS QSO halo masses is $\sim 3-6\times10^{12}\ h^{-1}\ M_\odot$ (specifically, $\left\langle \log(M_{\rm H}/h^{-1}\ M_\odot)\right\rangle = 12.80$ at $z = 1.5$ and 12.60 at $z = 3.5$, and 12.45 at $z = 4.5$). The scatters in the halo mass distributions are $\sim 0.3-0.5$ dex. The peak of the mass distribution of the BOSS QSOs is $\log(M_{\rm H}/h^{-1}\ M_\odot) \sim 12.40$, and the logarithmic mean of the BOSS QSO halo masses is 12.40 ($\sim 2\times10^{12}\ h^{-1}\ M_\odot$) at $z = 2.4$ (right panel). The typical halo mass of the BOSS QSOs is a factor of $\sim$ two times smaller than that of the SDSS QSOs at the same redshift ($\left\langle \log(M_{\rm H}/h^{-1}\ M_\odot)\right\rangle = 12.90$ at $z = 2.4$), and the standard deviation in the halo masses of the BOSS QSO is larger than that of the SDSS QSOs. The exact values of the peak and scatter of the halo mass distributions may depend on the detailed model parameters and may be affected by uncertainties in the model parameters. However, the difference in the halo mass distribution between the bright QSOs and the faint QSOs is intrinsic. The reasons for this difference are three fold: (1) the BOSS QSOs are ~ 2.5 magnitudes fainter (roughly an order of magnitude smaller in luminosity) than the SDSS QSOs, which results in a difference in the peak halo mass of ~ 0.5 dex; (2) the distribution of the halo masses is skewed toward the massive end and the resulting logarithmic mean of the halo masses is larger than the peak mass; and (3) the mass distribution for the host dark matter halos of

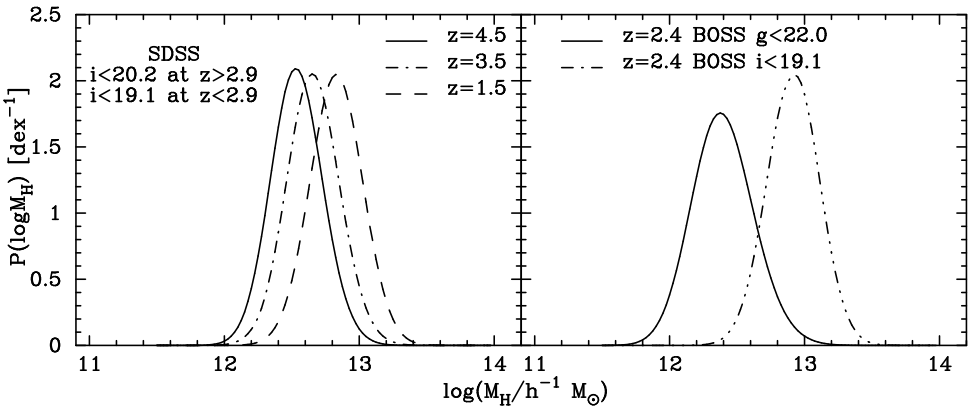

Fig. 4 The mass distribution of the host dark matter halos of QSOs at different redshifts. The left and right panels show the results obtained from the best fit QSO model for QSOs with a similar magnitude limit to that of the DR5 SDSS QSOs and BOSS QSOs, respectively. The solid, dash-dotted, and dashed lines in the left panel represent the halo mass distribution of those QSOs at redshift $z = 4.5, 3.5$, and 1.5, respectively. The corresponding logarithmic mean of the halo masses are $\left\langle \log(M_{\rm H}/h^{-1}\,M_\odot)\right\rangle = 12.45$ at $z = 4.5$, 12.60 at $z = 3.5$, and = 12.80 at $z = 1.5$. The solid line in the right panel shows the halo mass distribution for the BOSS QSOs at $z = 2.4$. For comparison, the dot-dot-dot-dashed line shows the halo mass distribution for those QSOs that can be detected at $z = 2.4$ if the magnitude limit is the same as the SDSS QSO survey. At redshift $z = 2.4$, the logarithmic mean of the halo masses is $\left\langle \log(M_{\rm H}/h^{-1}\,M_\odot)\right\rangle = 12.40$ for the BOSS QSOs, while it is 12.90 for those SDSS QSOs.

the less luminous BOSS QSOs is more extended with a standard deviation of ~ 0.5 dex compared with that of the SDSS QSOs with a standard deviation of ~ 0.4 dex), which also causes the resulting logarithmic mean of the halo masses to be larger than the peak mass. Therefore, the difference in linear biases estimated from these two QSO samples is also not so significant (the bias obtained from the BOSS QSOs is only ~ 0.5 smaller than that from the SDSS QSOs). The typical halo mass of the SDSS or BOSS QSOs estimated in this paper is consistent with those previous estimates, e.g., the minimum halo mass of the SDSS QSOs is $\sim (2-4)\times 10^{12}\ h^{-1}\ M_\odot$ and $(4-6)\times 10^{12}\ h^{-1}\ M_\odot$ at $2.9 \le z \le 3.5$ and $z \ge 3.5$, respectively (Shen et al. 2007); and the typical mass of the host halos of the BOSS QSOs is $\sim 2\times 10^{12}\ h^{-1}\ M_\odot$ at $z \sim 2.4$ (White et al. 2012). We also note here other estimates of the masses for halos that host QSOs in the literature, e.g., $\sim (3.0\pm 1.6)\times 10^{12}\ h^{-1}\ M_\odot$ over the redshift range of $0.3 < z < 2.9$ for the 2QZ QSOs with a limit of one magnitude fainter than the SDSS QSOs (Croom et al. 2005); $\sim 10^{12}\ h^{-1}\ M_\odot - 10^{13}\ h^{-1}\ M_\odot$ for the 2QZ QSOs by Porciani et al. (2004) (see also Porciani & Norberg 2006; Lidz et al. 2006). Considering the difference in the magnitude limits of different surveys, these estimates on the mass of halos that host QSOs are roughly consistent with those obtained from the QSO model in this paper.

As seen from Figure 1, the detected SDSS QSOs are at the high luminosity end of the QSO LFs and they are dominated by those MBH systems radiating at a rate close to their peak luminosity (see Eq. (9)). For a QSO population with luminosity one order of magnitude brighter than a faint QSO population, the masses of their host halos may also be a factor of four times or more larger than that of the faint population according to the relation between the MBH mass and the halo mass (Eq. (5)). Therefore, the linear bias of the bright population should be substantially larger than that of the faint population.

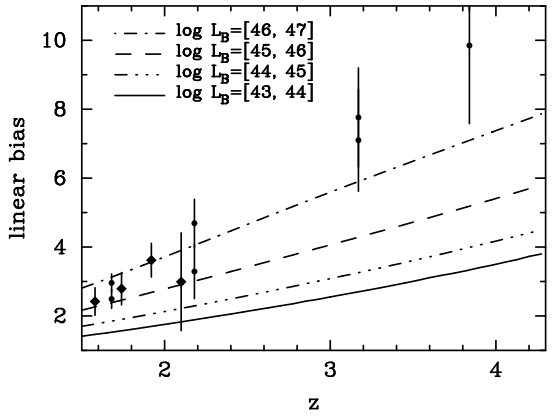

Fig. 5 Linear bias of QSOs in different luminosity ranges estimated from the best fit QSO model at different redshifts. From top to bottom, dot-dashed, dashed, dot-dot-dot-dashed and solid lines represent the results for those QSOs with the *B*-band luminosity in the range of $10^{46} - 10^{47}$, $10^{45} - 10^{46}$, $10^{44} - 10^{45}$ and $10^{43} - 10^{44}$erg s^{-1}, respectively. This figure shows a weak dependence of the linear bias on the QSO luminosity, especially at low redshift.

Figure 5 shows the linear biases obtained from our QSO model for QSOs of different luminosity ranges. Obviously there is a dependence of the linear bias on the QSO luminosity. However, this dependence is weaker than that inferred directly from Equation (13), mainly because of the scatters in the $M_{\bullet,\rm f} - M_{\rm H}$ relation and the BCs, and the evolution of luminosity for individual QSOs, which dilute the dependence of the linear bias on the QSO luminosity. This weak dependence is consistent with current observations (see Porciani & Norberg 2006; Myers et al. 2007; da Ângela et al. 2008; Shen et al. 2009).

4.3 The MBH Mass versus the Halo Mass

Figure 6 shows the relation between the MBH mass and the halo mass, as derived from the QSO model that best fits the QSO LF and which can explain the linear biases well. As seen from Figure 6, the $M_\bullet - M_{\rm H}$ relation required by the QSO model does not seem to be consistent with the observations for a number of lensing objects, for which both the MBH mass and the halo mass are estimated by Bandara et al. (2009; the squares). Part of the reason for this inconsistency might be that the low redshift AGNs investigated by Bandara et al. (2009) at redshift $z \sim 0.3$ are not triggered by major mergers of galaxies and dark matter halos. For comparison, the $M_\bullet - M_{\rm H}$ relation, obtained by Ferrarese (2002) for some nearby galaxies, is also shown in Figure 6. Different lines represent the resulting $M_\bullet - M_{\rm H}$ relation by relating the observed circular velocities $v_{\rm c,obs}$ of these galaxies to the virial velocities of their host halo $v_{\rm vir}$ (the solid, dashed and dot-dashed lines show the results represented by eqs. (4), (6) and (7) in Ferrarese 2002, respectively). The $M_\bullet - M_{\rm H}$ relation constrained by the QSO LFs in this paper is consistent with the one obtained by Ferrarese (2002) at the low mass end, for which $v_{\rm c,obs} = 1.8 v_{\rm vir}$ is adopted (the dot-dashed line in Fig. 6). However, the halo mass $M_{\rm H}$ in Equation (2) is the mass of the halo resulting from a major merger at redshift z, which may be significantly different from the host halo mass for nearby quiescent MBHs, since the resulting halo can significantly grow over the intervening time, but their central MBH cannot. For a halo with mass of $\sim 10^{12} M_\odot$ at redshift $z = 1.5$, for example, it may grow to a halo at $z = 0$ with mass two times larger (see Wechsler et al. 2002; Zhao et al. 2009). Therefore, the $M_{\bullet,\rm f} - M_{\rm H}$ relation required by

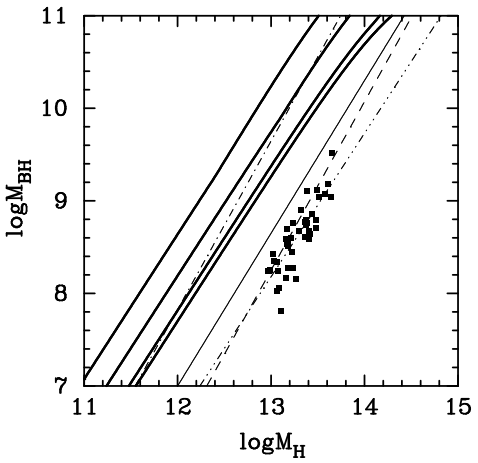

Fig. 6 The $M_\bullet - M_{\rm H}$ relation. The thick solid curves represent the $M_\bullet - M_{\rm H}$ relation constrained by the QSO model in this paper at redshift $z = 4, 3, 2$ and 1 (from top to bottom), respectively. The squares are the objects from Bandara et al. (2009), for which the MBH masses are estimated by using the empirical relations, and the halo masses are estimated by using the gravitational lensing technique. The thin solid, dashed and dot-dashed lines represent the estimated $M_\bullet - M_{\rm H}$ relation at $z = 0$ as described by equations (4), (6) and (7) in Ferrarese (2002), respectively. The thin dot-dot-dot-dashed line represents the estimated $M_\bullet - M_{\rm H}$ relation at $z \sim 0.1 - 0.3$ by Bandara et al. (2009).

the QSO LFs in our model may only represent the upper bound of the $M_\bullet - M_{\rm H}$ relation for nearby MBHs and could shift towards the solid line and dashed line shown in Figure 6. We conclude that the $M_{\bullet,{\rm f}} - M_{\rm H}$ relation constrained by the QSO model in this paper is compatible with current estimates on the $M_\bullet - M_{\rm H}$ relation at low redshift (see Ferrarese 2002 and Bandara et al. 2009).

5 CONCLUSIONS

We constructed a simple QSO model in this paper to study the clustering and the properties of the host dark matter halos of QSOs by adopting the major merger hypothesis, i.e., the major merger of dark matter halos can lead to the nuclear activities in the centers of the halos after merging. After the triggering of nuclear activity in halos, the evolution of the disk accretion of the central MBHs is assumed to generally follow two phases, i.e., the active MBHs accrete material (1) first via a constant Eddington ratio ($\lambda \sim 0.3$) as the initial supply is plentiful and the accretion is self-regulated; and (2) then via a rate declining with time as a power law because of the declining supply of available material or the long term evolution of the disk. The final mass of an MBH in a dark matter halo after the merger is assumed to be related to its host halo's mass due to feedback from the nuclear activity. We use an MCMC method to first calibrate the QSO model by fitting the HXLFs obtained from observations. Adopting the calibrated model parameters, we find that the OLF can also be well matched by the QSO model. We then use the QSO model that best fits the HXLFs and OLFs to estimate the linear biases of QSOs at different luminosity and redshift by accounting for the magnitude limits of different QSO surveys, and we find the linear biases estimated from the SDSS QSOs and the BOSS QSOs can be well reproduced by the model. The typical mass of the SDSS QSOs at redshift $1.5 < z < 4.5$ is $\sim (3 - 6) \times 10^{12}\ h^{-1}\ M_\odot$ and the typical mass of the BOSS QSOs at $z \sim 2.4$ is $\sim 2 \times 10^{12}\ h^{-1}\ M_\odot$. For relatively faint QSOs, the mass distribution of their host dark matter halos is wide compared with that of bright QSOs because faint QSOs can be hosted in both

big halos and smaller halos but bright QSOs are only hosted in big halos, which is part of the reason for the weak dependence of the model's predicted linear biases on the QSO luminosity. Future QSO surveys may accurately measure the linear bias of QSOs as a function of luminosity and redshift, which may provide strong constraints on the properties of the QSO host dark matter halos and thus the formation and evolution of QSOs.

Acknowledgements We thank the anonymous referee for helpful comments. We thank Prof. Qingjuan Yu for numerous discussions. This work was supported in part by the National Natural Science Foundation of China (Grant Nos. 10973017 and 11033001), and the 100 Talents Program from the National Astronomical Observatories, Chinese Academy of Sciences.

References

Aird, J., Nandra, K., Laird, E. S., et al. 2010, MNRAS, 401, 2531
Bahcall, J. N., Kirhakos, S., Saxe, D. H., & Schneider, D. P. 1997, ApJ, 479, 642
Bandara, K., Crampton, D., & Simard, L. 2009, ApJ, 704, 1135
Barger, A. J., Cowie, L. L., Mushotzky, R. F., et al. 2005, AJ, 129, 578
Bongiorno, A., Zamorani, G., Gavignaud, I., et al. 2007, A&A, 472, 443
Booth, C. M., & Schaye, J. 2010, MNRAS, 405, L1
Brown, M. J. I., & the Boötes Field Collaborations 2010, in IAU Symp. 262, eds. G. Bruzual, & S. Charlot, 244 (arXiv:1001.2368)
Carlberg, R. G. 1990, ApJ, 350, 505
Croom, S. M., Smith, R. J., Boyle, B. J., et al. 2004, MNRAS, 349, 1397
Croom, S. M., Boyle, B. J., Shanks, T., et al. 2005, MNRAS, 356, 415
Croom, S. M., Richards, G. T., Shanks, T., et al. 2009, MNRAS, 399, 1755
Croton, D. J., Springel, V., White, S. D. M., et al. 2006, MNRAS, 365, 11
da Ângela, J., Shanks, T., Croom, S. M., et al. 2008, MNRAS, 383, 565
Duffy, A. R., Schaye, J., Kay, S. T., & Dalla Vecchia, C. 2008, MNRAS, 390, L64
Ebrero, J., Carrera, F. J., Page, M. J., et al. 2009, A&A, 493, 55
Eke, V. R., Cole, S., Frenk, C. S., & Patrick Henry, J. 1998, MNRAS, 298, 1145
Fabian, A. C. 1999, MNRAS, 308, L39
Fakhouri, O., & Ma, C.-P. 2008, MNRAS, 386, 577
Fakhouri, O., Ma, C.-P., & Boylan-Kolchin, M. 2010, MNRAS, 406, 2267
Ferrarese, L. 2002, ApJ, 578, 90
Ferrarese, L., & Merritt, D. 2000, ApJ, 539, L9
Gebhardt, K., Bender, R., Bower, G., et al. 2000, ApJ, 539, L13
Genel, S., Genzel, R., Bouché, N., et al. 2008, ApJ, 688, 789
Genel, S., Genzel, R., Bouché, N., Naab, T., & Sternberg, A. 2009, ApJ, 701, 2002
Greene, J. E., Ho, L. C., & Barth, A. J. 2008, ApJ, 688, 159
Haiman, Z., & Hui, L. 2001, ApJ, 547, 27
Hasinger, G. 2008, A&A, 490, 905
Hernquist, L. 1989, Nature, 340, 687
Hopkins, P. F., & Hernquist, L. 2006, ApJS, 166, 1
Hopkins, P. F., Richards, G. T., & Hernquist, L. 2007, ApJ, 654, 731
Hopkins, P. F., Hernquist, L., Cox, T. J., & Kereš, D. 2008, ApJS, 175, 356
Jin, C., Ward, M., & Done, C. 2012, MNRAS, 425, 907
Jing, Y. P. 1998, ApJ, 503, L9
Kauffmann, G., & Haehnelt, M. 2000, MNRAS, 311, 576
King, A. 2003, ApJ, 596, L27

Kollmeier, J. A., Onken, C. A., Kochanek, C. S., et al. 2006, ApJ, 648, 128
La Franca, F., Fiore, F., Comastri, A., et al. 2005, ApJ, 635, 864
Lacey, C., & Cole, S. 1994, MNRAS, 271, 676
Lidz, A., Hopkins, P. F., Cox, T. J., Hernquist, L., & Robertson, B. 2006, ApJ, 641, 41
Lynden-Bell, D. 1969, Nature, 223, 690
Malbon, R. K., Baugh, C. M., Frenk, C. S., & Lacey, C. G. 2007, MNRAS, 382, 1394
Martini, P., & Weinberg, D. H. 2001, ApJ, 547, 12
Murray, N., Quataert, E., & Thompson, T. A. 2005, ApJ, 618, 569
Myers, A. D., Brunner, R. J., Nichol, R. C., et al. 2007, ApJ, 658, 85
Parkinson, H., Cole, S., & Helly, J. 2008, MNRAS, 383, 557
Porciani, C., Magliocchetti, M., & Norberg, P. 2004, MNRAS, 355, 1010
Porciani, C., & Norberg, P. 2006, MNRAS, 371, 1824
Richards, G. T., Strauss, M. A., Fan, X., et al. 2006, AJ, 131, 2766
Ross, N. P., Shen, Y., Strauss, M. A., et al. 2009, ApJ, 697, 1634
Salpeter, E. E. 1964, ApJ, 140, 796
Shen, Y. 2009, ApJ, 704, 89
Shen, Y., Strauss, M. A., Oguri, M., et al. 2007, AJ, 133, 2222
Shen, Y., Strauss, M. A., Ross, N. P., et al. 2009, ApJ, 697, 1656
Sheth, R. K., Mo, H. J., & Tormen, G. 2001, MNRAS, 323, 1
Sheth, R. K., & Tormen, G. 1999, MNRAS, 308, 119
Silk, J., & Rees, M. J. 1998, A&A, 331, L1
Silverman, J. D., Green, P. J., Barkhouse, W. A., et al. 2008, ApJ, 679, 118
Small, T. A., & Blandford, R. D. 1992, MNRAS, 259, 725
Somerville, R. S., Hopkins, P. F., Cox, T. J., Robertson, B. E., & Hernquist, L. 2008, MNRAS, 391, 481
Tinker, J. L., Robertson, B. E., Kravtsov, A. V., et al. 2010, ApJ, 724, 878
Tremaine, S., Gebhardt, K., Bender, R., et al. 2002, ApJ, 574, 740
Ueda, Y., Akiyama, M., Ohta, K., & Miyaji, T. 2003, ApJ, 598, 886
Vasudevan, R. V., & Fabian, A. C. 2009, MNRAS, 392, 1124
Wechsler, R. H., Bullock, J. S., Primack, J. R., Kravtsov, A. V., & Dekel, A. 2002, ApJ, 568, 52
White, M., Myers, A. D., Ross, N. P., et al. 2012, arXiv: 1203.5306
Yencho, B., Barger, A. J., Trouille, L., & Winter, L. M. 2009, ApJ, 698, 380
York, D. G., Adelman, J., Anderson, J. E., Jr., et al. 2000, AJ, 120, 1579
Yu, Q., & Lu, Y. 2004, ApJ, 602, 603
Yu, Q., & Lu, Y. 2008, ApJ, 689, 732
Yu, Q., Lu, Y., & Kauffmann, G. 2005, ApJ, 634, 901
Yu, Q., & Tremaine, S. 2002, MNRAS, 335, 965
Zhao, D. H., Jing, Y. P., Mo, H. J., & Börner, G. 2009, ApJ, 707, 354